# Microstructural Crimp of the Lamina Cribrosa and Peripapillary Sclera Collagen Fibers

Ning-Jiun Jan,[1–4] Celeste Gomez,[1] Saundria Moed,[1] Andrew P. Voorhees,[2–4] Joel S. Schuman,[2–5] Richard A. Bilonick,[2] and Ian A. Sigal[1–4]

[1]Department of Bioengineering, Swanson School of Engineering, University of Pittsburgh, Pennsylvania, United States
[2]Department of Ophthalmology, University of Pittsburgh School of Medicine, Pittsburgh, Pennsylvania, United States
[3]McGowan Institute for Regenerative Medicine, University of Pittsburgh School of Medicine and University of Pittsburgh, Pittsburgh, Pennsylvania, United States
[4]The Louis J. Fox Center for Vision Restoration of UPMC and the University of Pittsburgh, Pittsburgh, Pennsylvania, United States
[5]NYU Langone Eye Center, New York University, New York, New York, United States

Correspondence: Ian A. Sigal, Laboratory of Ocular Biomechanics, Department of Ophthalmology, University of Pittsburgh Medical Center, 203 Lothrop Street, Eye and Ear Institute, Room 930, Pittsburgh, PA 15213, USA; ian@OcularBiomechanics.com.

Submitted: March 4, 2017
Accepted: May 16, 2017

Citation: Jan N-J, Gomez C, Moed S, et al. Microstructural crimp of the lamina cribrosa and peripapillary sclera collagen fibers. *Invest Ophthalmol Vis Sci*. 2017;58:3378–3388. DOI: 10.1167/iovs.17-21811

**Purpose.** Although collagen microstructural crimp is a major determinant of ocular biomechanics, no direct measurements of optic nerve head (ONH) crimp have been reported. Our goal was to characterize the crimp period of the lamina cribrosa (LC) and peripapillary sclera (PPS) at low and normal IOPs.

**Methods.** ONHs from 11 sheep eyes were fixed at 10-, 5-, or 0-mm Hg IOP and crimp periods measured manually from coronal cryosections imaged with polarized light microscopy (PLM). Using linear mixed-effect models, we characterized the LC and PPS periods, and how they varied with distance from the scleral canal edge.

**Results.** A total of 17,374 manual collagen crimp period measurements were obtained with high repeatability (1.9 μm) and reproducibility (4.7 μm). The periods were smaller ($P < 0.001$) and less variable in the LC than in the PPS: average (SD) of 13.8 (3.1) μm in the LC, and 31.0 (10.4) μm in the PPS. LC crimp period did not vary with distance from the scleral canal wall ($P > 0.1$). PPS period increased with the square root of the distance to the canal ($P < 0.0001$).

**Conclusions.** Small, uniform crimp periods within the sheep LC and immediately adjacent PPS may indicate that these tissues are setup to prevent large or heterogeneous deformations that insult the neural tissues within the canal. An increasing more variable period with distance from the canal provides a smooth transition of mechanical properties that minimizes stress and strain concentrations.

Keywords: optic nerve head, collagen, biomechanics, lamina cribrosa, sclera, peripapillary sclera, scleral canal, sheep

Collagen is the main load-bearing component of soft tissues, including the eye. The organization and hierarchical architecture of collagen fibers determine tissue mechanical behavior, including key tissue properties, such as anisotropy (directional stiffness) and nonlinearity (strain-dependent stiffness).[1] The influence of fiber architecture is often stronger than that of the chemical composition of the fibers.[1–4] Several recent studies have addressed the overall organization and orientation of collagen in the eye, focusing on the corresponding tissue anisotropy.[5–8] However, the microstructural characteristics of the collagen fibers and their role in eye tissue nonlinearity remain relatively poorly understood. In other soft tissues, it is well understood that their nonlinear behavior is largely driven by the micrometer-scale waviness, or crimp, of the collagen fibers.[9,10] Studies in tendon and skin, for example, have demonstrated an important interrelationship between crimp and mechanical properties in health, aging, and disease.[11–13]

In the eye, studies have been limited to observations of fiber waviness and undulations in images acquired with a diversity of techniques, including brightfield,[14] electron,[15] and nonlinear microscopy,[6,16–18] and magnetic resonance imaging (MRI),[19] or to estimates of crimp properties from inverse numerical models.[20–22] Employing transmission electron microscopy Liu and colleagues[23] measured collagen fiber crimp in the cornea. The numerical models point to collagen crimp characteristics playing a critical role in eye biomechanics.[20–23] Nevertheless, no systematic experimental quantifications of posterior pole micrometer-scale collagen crimp have been reported.

Our goal was to quantify collagen fiber crimp in the lamina cribrosa (LC) and surrounding peripapillary sclera (PPS), compare crimp distribution between these tissues, and analyze how collagen crimp varies with distance from the scleral canal. This information will enable the development of more realistic models of ocular tissue biomechanics. Further, this study will provide a basis to understand the underlying mechanisms by which microstructure governs larger scale mechanics of soft tissues, as well as the role of microstructure on eye physiology, aging, and in biomechanics-related diseases, such as glaucoma.

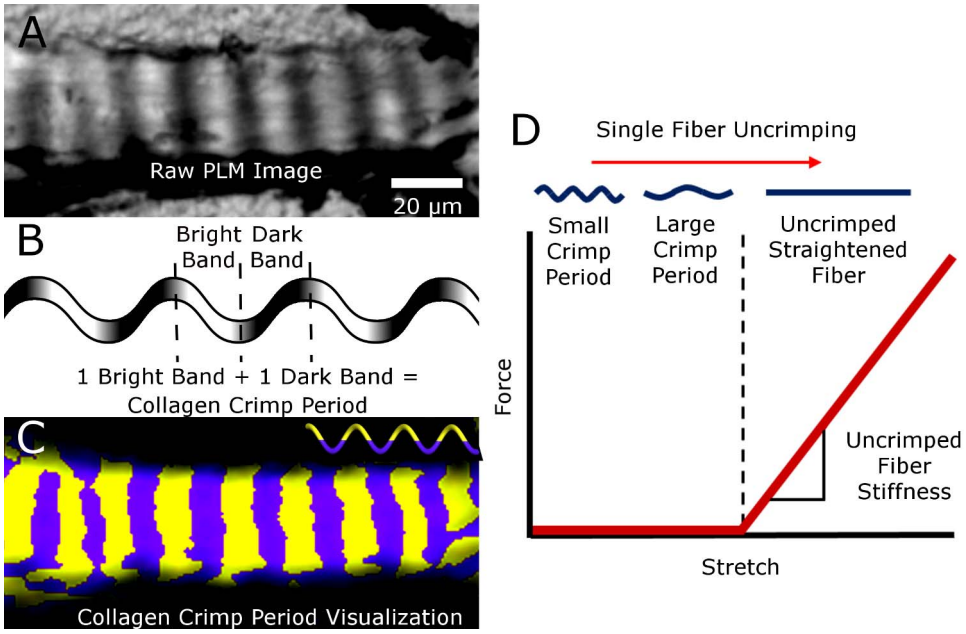


**Figure 1.** The collagen crimp period visualized using PLM. A LC trabeculae beam appears banded when imaged with PLM (**A**). Adding the lengths of one bright band and one dark band makes one collagen crimp period (**B**). From processing the raw PLM images, we can pseudocolor half periods as alternating yellow and purple bands to visualize the crimp period (**C**). As a single fiber stretches it uncrimps, with relatively little force until it loses all crimp. The straightened fiber can only be stretched further by making the fiber longer, which requires an increasing force, and so the fiber appears stiff (**D**).

## Methods

One of the most natural characteristics of collagen fiber crimp is the length of a wave, or its period (Fig. 1). In this first study, we characterized the distribution of the crimp period in the collagen fibers of the LC and PPS from sheep ONHs fixed at low IOPs.

### Specimen Preparation

Six adult sheep eyes approximately 2-years old were acquired from a local abattoir and processed within 24 hours of death. Using scalpels, razors, and forceps, the muscles, fat, and episcleral tissues were removed from each eye. The eyes were cannulated through the anterior chamber to set the IOP using a fluid column. We characterized the crimp period at normal (10 mm Hg),[24] subphysiologic (5 mm Hg), and zero (0 mm Hg) IOPs. Two eyes were fixed at each pressure. All eyes were immersion fixed with 10% formalin for at least 12 hours while maintaining pressure. After fixation, the ONHs were excised using an 11.5-mm diameter trephine and cryosectioned into 30-μm thick coronal sections. For each eye, at least three sections at the level of the LC and three at the level of the PPS were selected for analysis. Sections were selected when they were free of artifacts, such as folds. Due to the natural eye-to-eye variability in LC position within the canal, as well as tilt during sectioning, some sections were not ideal for both tissues. A total of 26 sections were selected for analysis.

### Imaging and Data Acquisition

The selected sections were imaged with PLM using previously reported methods[25,26] in order to visualize the collagen crimp period (Fig. 1). Briefly, two filters (Hoya, Tokyo, Japan) were used with the polarizer filter placed before the sample and the analyzer filter placed after the sample. Images at multiple filter

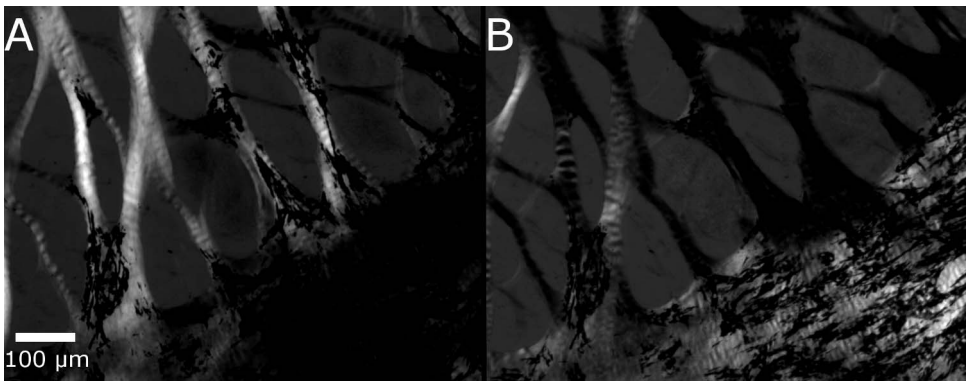


**Figure 2.** The same region of the ONH, imaged with two different polarized filter orientations, 45° apart. Multiple filter orientations were used in order to visualize the collagen crimp period in bundles oriented in different directions. In this case, the crimps in some LC bundles were more distinct in (**A**), whereas those in the PPS were more distinct in (**B**).

orientations 45° apart were captured for optimal crimp period visualization (Fig. 2). Up to four filter orientations were used in each section to quantify collagen crimp period. An Olympus SZX16 microscope was used with an Olympus DP80 camera (36-bit, RGB, pixel shift setting), a 0.6× reducer, and 0.8× objective (numerical aperture [NA], 0.12; Olympus, Tokyo, Japan). A manual stage was used to capture images with 20% overlap, which were then stitched into mosaics using FIJI Is Just ImageJ (FIJI).[27,28] To image the fine details of the LC, the 11.5× magnification setting on the microscope was used (0.37 μm/pixel). For each section of LC, 10 to 30 images were captured in order to visualize the whole LC and the scleral canal. The PPS sections were imaged using the 4× magnification setting (1.08 μm/pixel). The PPS is much larger and it would have been very time consuming to manually capture and stitch the hundreds of images that would have resulted from imaging at high magnification. For each section of PPS, 20 to 40 images were sufficient to visualize the whole tissue section. We have previously shown that measurements derived from intensity in PLM images are robust to changes in imaging system and magnification.[25] In the next subsection we describe the test used to verify that magnification choice did not affect the measured collagen crimp period.

## Measuring Collagen Crimp Period

Using FIJI,[28] the crimp period was manually measured from PLM images, akin to previously reported methods (Fig. 1).[29] From the PLM images, the period was measured manually by identifying the inflection points between the bright and dark bands, where each band corresponds to half of a crimp period. A straight line was used to measure the length of three sequential crimp periods by identifying three bright and dark bands. This length was divided by 3 to get the average crimp period.

Due to the large number of manual measurements required, the work was split between several markers. To determine the repeatability and reproducibility of measuring the collagen crimp period, one section of the ONH fixed at 5-mm Hg IOP was imaged (12-bit, grayscale) using a Nikon Eclipse Ti microscope (Nikon, Melville, NY, USA) coupled with a Cascade camera (Roper Scientific, Sarasota, FL, USA) and 10× objective (NA, 0.5, 0.80 μm/pixel). Nine markers delineated the same 34 fiber bundles in the image three times each.

To verify that collagen crimp period measurements are robust to acquisition magnification, one section of the ONH fixed at 5-mm Hg IOP was imaged using several magnification of the Olympus SZX16 microscope coupled with the Olympus DP80 camera, 0.6× reducer, and 0.8× objective (NA, 0.12), discussed above. A total of eight magnification settings were used to capture this series of images of a LC (2.5× with 1.75 μm/pixel through 11.5× with 0.37 μm/pixel). Below 2.5×, the collagen crimp period of the LC was no longer discernible, and 11.5× was the highest setting on the microscope. Ten fiber bundles were identified in these images from different magnification settings and the collagen crimp period was measured in each bundle.

To confirm that the collagen crimp period distributions were robust to changes in imaging setup, we used alternative setups with different microscope–camera pairings to image the same sections of the two sheep eyes above fixed at 5-mm Hg IOP. Sections through the LC were imaged (12-bit grayscale, 0.73 μm/pixel) using a 10× objective (NA, 0.3) on an Olympus BX60 microscope. This microscope was paired with an RT Slider camera (SPOT Imaging Solutions, Sterling Heights, MI, USA). Sections through the PPS were imaged using the Nikon-Cascade microscope-camera pair with the same settings as previously described above (in paragraph detailing the repeatability and reproducibility tests). The LC and PPS collagen crimp periods were measured and the resulting distributions compared with those previously obtained from images acquired using the Olympus–Olympus microscope–camera pair.

To confirm that the collagen crimp period measurements obtained from two eyes are representative of a larger population of eyes, we repeated the measurements in an additional five eyes fixed at 5-mm Hg IOP, for a total pool of seven eyes from four animals. Collagen crimp period was measured in the LC and PPS regions using images taken using the alternative setup described above, and the resulting distributions were compared between animals and between eyes.

## Measuring Distance From the Scleral Canal

To evaluate how the collagen crimp period changed with distance from the scleral canal, a border between the LC and the PPS was manually drawn for each section. Measurements inside this border were categorized as on LC, whereas the measurements outside this border were categorized as on PPS. The distance of a period measurement to the canal border was calculated using custom scripts as the shortest distance between the center of each line segment used for crimp period measurement and the manually delineated canal border.

## Crimp Period Visualization

Some PLM images were further processed to better visualize the collagen crimp period in all fiber bundle directions simultaneously. This was done purely for visualization purposes, not for measurement. Using previously reported methods,[25,26] we processed the images to determine pixel-by-pixel collagen fiber orientation information. This information was then used to find the difference between each pixel's fiber orientation, and the average fiber orientation in its neighborhood (10-μm radius). We then pseudocolored each pixel purple, if this difference was positive, or yellow, if this difference was negative. With this processing, crimp is easily discernible as purple and yellow bands (Fig. 1) orientation. Without this processing, crimp period visibility depends on the relative orientation of the collagen bundle and the polarized light filters.

## Statistical Analyses

**Repeatability and Reproducibility of Collagen Crimp Period Measurements.** To evaluate the repeatability within each marker, the SD of each marker's three crimp period measurements was calculated for each fiber bundle. To evaluate reproducibility across the group of markers, the SD across all marker collagen crimp period measurements for each fiber bundle was calculated.

**Robustness of Collagen Crimp Period Measurements Across Magnifications.** To evaluate the robustness across magnifications, the SD of crimp period measurements from different magnifications was calculated for each fiber bundle.

**Robustness of Collagen Crimp Period Measurements to Changes in Imaging Setups.** Linear mixed-effect models accounting for autocorrelation of measurements from the same section, eye, and animal were used to test for differences in crimp period measurements between those from the standard versus alternative imaging setups.

**Confirming Measurements are Representative of a Larger Population.** From the measurements pooled across seven eyes from four animals, all fixed at 5 mm Hg, linear mixed-effect models accounting for autocorrelation of mea-

surements from the same section were used to test if measurements were significantly different between those from different eyes and animals.

**Collagen Crimp Period Distribution.** The collagen crimp period distributions in the LC and PPS were calculated. In addition, to compare the collagen crimp period of these two regions, a linear mixed-effect model accounting for autocorrelation of measurements from the same section, eye, animal, and IOP was used.

**Spatial Distribution of the Collagen Crimp Period.** To determine the spatial distribution of the collagen crimp period in the LC and the PPS the collagen crimp period was first separated into groups based on spatial distance from the scleral canal. To further understand the variations in PPS crimp period with distance from the canal edge, we separated the PPS crimp period measurements into two categories: proximal (≤500 μm from the scleral canal) and distal (>500 μm from the scleral canal). Linear mixed-effect models accounting for autocorrelation of measurements from the same section, eye, animal, and IOP were used to determine if the PPS crimp period in these two regions were different from each other, and whether they were different from the LC crimp period. Next, linear mixed-effect models accounting for autocorrelation of measurements from the same section, eye, animal, and IOP were used to find associations between collagen crimp period and radial distance from the scleral canal. The measurements from the LC and PPS were analyzed separately to determine if the collagen crimp period in each region was associated with distance from the scleral canal. When visualizing the results, we suspected that the relationship between PPS crimp period and distance from the canal was not linear. To determine the best fit, several models were fit with distance transformations (no transform or linear, logarithmic, and square root), and the model with the lowest Akaike Information Criterion (AIC) chosen. The AIC is a measure that determines the quality of the model by evaluating the tradeoff between goodness of fit and model complexity. It is important to note the AIC does not determine the significance of the model, only a relative quality of the model compared with other models of the same data.

## Results

A total of 17,374 manual collagen crimp period measurements were made in this study. Repeated measurements made by a marker had a maximum SD of 1.9 μm across the 34 fiber bundles (Fig. 3A). Reproducibility of measurements between markers had a maximum SD of 4.7 μm across the 34 bundles (Fig. 3B). Comparing measurements of collagen crimp period from images acquired with a range of magnifications between 2.5× and 11.5× the largest SD was 0.4 μm across 10 fiber bundles (Fig. 4). Measurements were not significantly different when using different microscope-camera pairs ($P > 0.1$), nor were the measurements significantly different between those from different eyes and animals ($P > 0.1$, 7 eyes from 4 animals, 12,796 total measurements; Fig. 5).

To quantify the crimp period in different regions of the ONH, a total of 4498 manual measurements were taken, with at least 450 measurements in each of the 6 eyes. The collagen crimp period distributions between all eyes were similar (Fig. 6), with no significant differences between eyes fixed at the three IOPs (Fig. 7). There were no statistically significant differences in crimp period between eyes fixed at IOPs of 0-, 5-, or 10-mm Hg ($P > 0.1$). For every eye and IOP the crimp periods in the LC were significantly smaller ($P < 0.001$) and less variable ($P < 0.001$) than crimp periods in the PPS (Figs. 6, 7). When pooling crimp period measurements from all pressures, the average (SD) crimp period in the LC was 13.8 (3.1) μm, and 31.0 (10.4) μm in the PPS. The median crimp period in the LC was 13.3 μm, and 30.1 μm in the PPS. The crimp period ranges were 5.2 to 30.0 μm in the LC and 7.3 to 72.0 μm in the PPS.

In the LC, the crimp period did not vary significantly with distance from the scleral canal wall ($P > 0.1$). However, crimp period in the PPS had an interesting pattern (Fig. 8), being smallest next to the canal wall – and the LC, and increasing with distance from the canal wall. The crimp period in the proximal PPS (500 μm of PPS closest to the canal) had average (SD) of 22.4 (5.8) μm, which was significantly larger ($P < 0.001$) than the 13.8 (3.1) μm average (SD) crimp period in the LC, and significantly smaller than the 35.4 (9.5) μm average (SD) crimp period in the distal PPS (more than 500 μm away from the canal wall). The median crimp period in the proximal PPS was 21.6 μm, and 34.7 μm for the distal PPS. The increases in PPS crimp period magnitude and variability with distance from the canal wall were also significant ($P < 0.001$) and substantial, with period more than doubling in magnitude at 2 mm from the canal (Fig. 7).

All three models (linear – no transformation, log of distance, square-root of distance), showed a statistically significant association between crimp period and distance from the canal in the PPS ($P < 0.001$). The root-square model had the lowest AIC value (Table).

## Discussion

We have presented a detailed characterization of the collagen fiber crimp period in the LC and PPS at normal and low IOPs. To the best of our knowledge, this is the first systematic quantification of collagen fibers crimp properties in the posterior pole. The manual crimp period measurements were repeatable and reproducible both within and between markers. The measurements were robust to differences in the magnification used during image acquisition and to the use of different imaging setups with different microscope–camera pairings.

We quantified the collagen crimp period in the LC and PPS in eyes at normal and low IOPs. Three main results arise from this work: first, the collagen crimp period in the LC was smaller, and less variable, than the crimp period in the PPS, and did not change with distance from the canal. Second, there were no significant differences in collagen fiber crimp period in eyes fixed at IOPs of 0-, 5-, or 10-mm Hg. Third, in the proximal PPS, the collagen crimp period was slightly larger than in the LC, and increased nonlinearly with distance from the canal wall. Let us consider each of these in turn:

1. The collagen crimp period in the LC was smaller and less variable than the crimp period in the PPS, and did not vary with distance from the canal. This indicated that the baseline crimp period in the LC was uniform. Uniform crimp morphology has been hypothesized to have a steeper (or less gradual) stiffening response to stretch than variable crimp morphology (Fig. 9).[29] This means that the LC may have close to a step-wise stiffening response to stretch compared with the PPS. As the LC houses delicate retinal ganglion cell axons and astrocytes, this collagen crimp period distribution allows the whole LC to stiffen simultaneously, rather than allowing some parts to stiffen before others. This results in a more even response to changes in pressure across the whole LC in order to avoid concentrations of strain that could hurt the axons. Note that this still allows for local variations in IOP-induced deformations arising from the complex LC pore and beam architecture.[30,31]

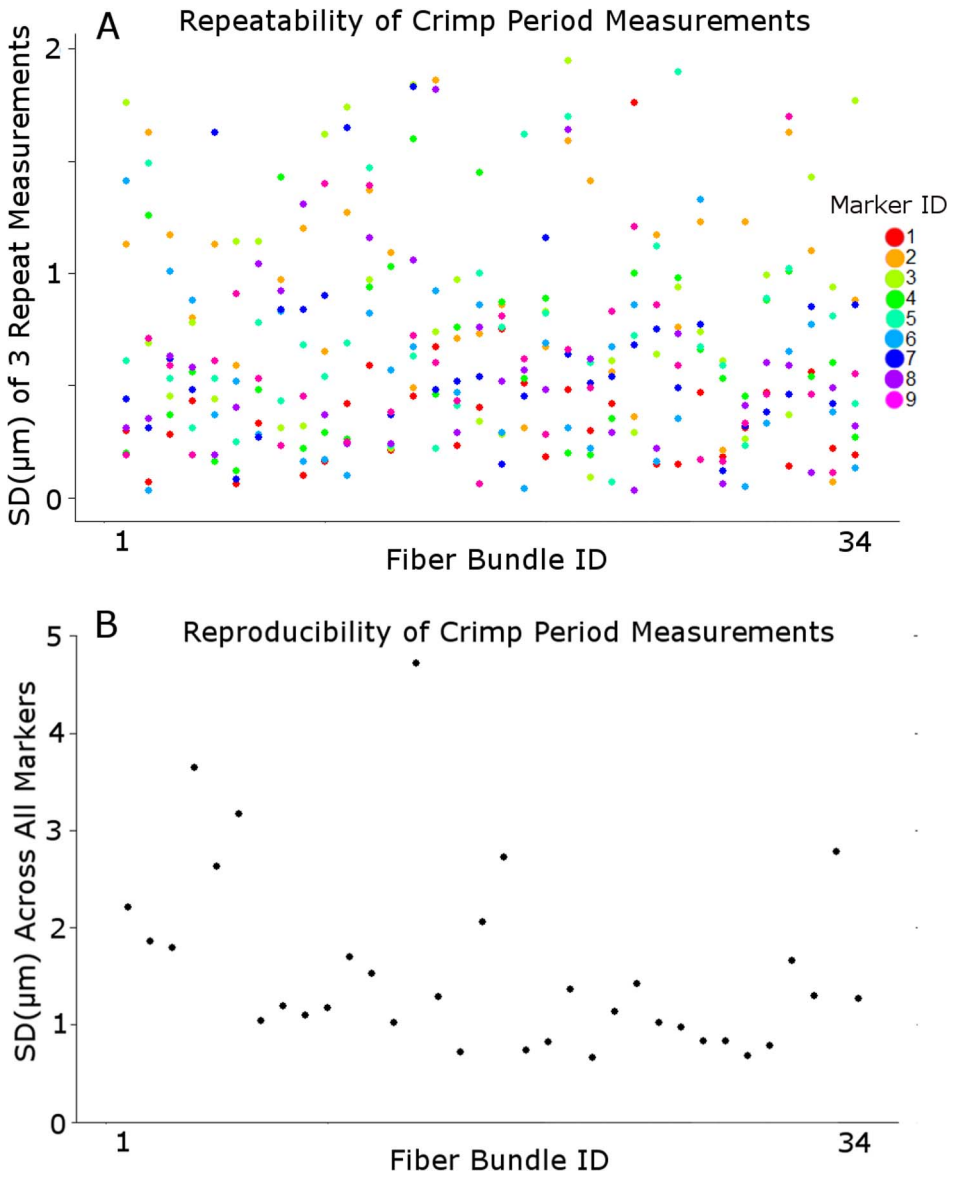


FIGURE 3. The repeatability (**A**) and reproducibility (**B**) of our manual collagen crimp period measurements. A total of nine individual markers measured the period in 34 fiber bundles three times to calculate the variability within (repeatability) and between (reproducibility) markers. Naturally, whether the repeatability and reproducibility are large or small, requires considering other measurements, such as those in Figures 6 and 7.

2. There were no significant differences in collagen fiber crimp period between eyes fixed at IOPs of 0-, 5-, or 10-mm Hg. We chose to study crimp period at these pressures to establish the baseline characteristics of the collagen fibers, without the potentially individual-specific effects of elevated IOP. From a mechanical perspective it would be anticipated that increases in IOP would cause collagen fiber stretch, affecting the fiber crimp characteristics.[32] Our results are important because they demonstrate that crimp period remains essentially unchanged when IOP decreases from physiologic to subphysiologic, and even to zero. These results are consistent with the mechanical concept that at low IOP, the collagen fibers bear little load, although there may still be residual stresses in the tissue.[33] Note that these results do not imply that there were no changes in crimp with increased IOP, only that there were no changes in crimp period. IOP may result in changes in other aspects of collagen crimp.
3. In the proximal PPS, the collagen crimp period was slightly larger than in the LC, and increased nonlinearly with distance from the canal wall. The baseline crimp period in the PPS was not uniform, indicating that the collagen fiber morphology is more variable in the PPS than in the LC. As mentioned above, the more heterogeneous the crimp morphology is at baseline, the more gradual the stiffening of the tissue is in response to stretch.[29] (Fig. 9). Thus, our finding of heterogeneous baseline PPS crimp is consistent with the nonlinear response to mechanical loading that is well recognized in the sclera.[34] Based on the finding that PPS crimp period increased with distance from the canal, we predict that scleral mechanical nonlinearity will also vary with distance from the canal. This would be in addition to the already known differences in anisotropy with

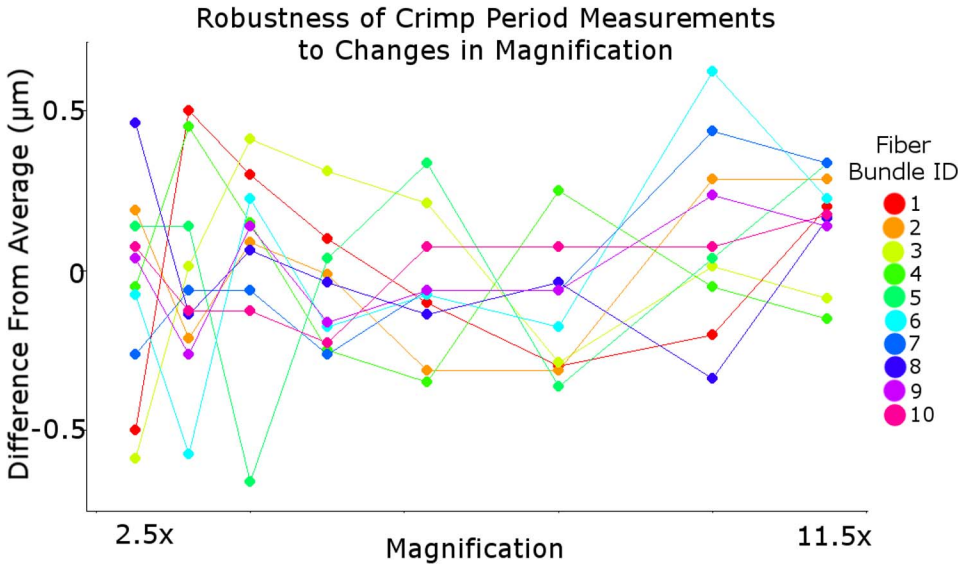


**Figure 4.** The robustness of our manual crimp period measurements to changes in image magnification. One individual measured the crimp period of 10 fiber bundles through eight magnification settings. Each crimp period measurement was subtracted from the average measurement for that bundle through the different magnifications in order to visualize the robustness. To understand whether the robustness to changes in image magnification is large or small, comparison with the actual measurements in Figures 6 and 7 is needed.

circumferential fibers in the proximal PPS.[26] To the best of our knowledge, experiments have not yet been able to determine this. From a mechanical perspective, the canal opening in the scleral shell will result in the circumferential stresses being maximal at the canal edge, and decrease with distance from the canal. In a homogeneous thin shell, this decrease is proportional to the inverse of the square of the distance from the canal.[35] The pattern of crimp properties observed could function to counterbalance these stress concentrations. In this

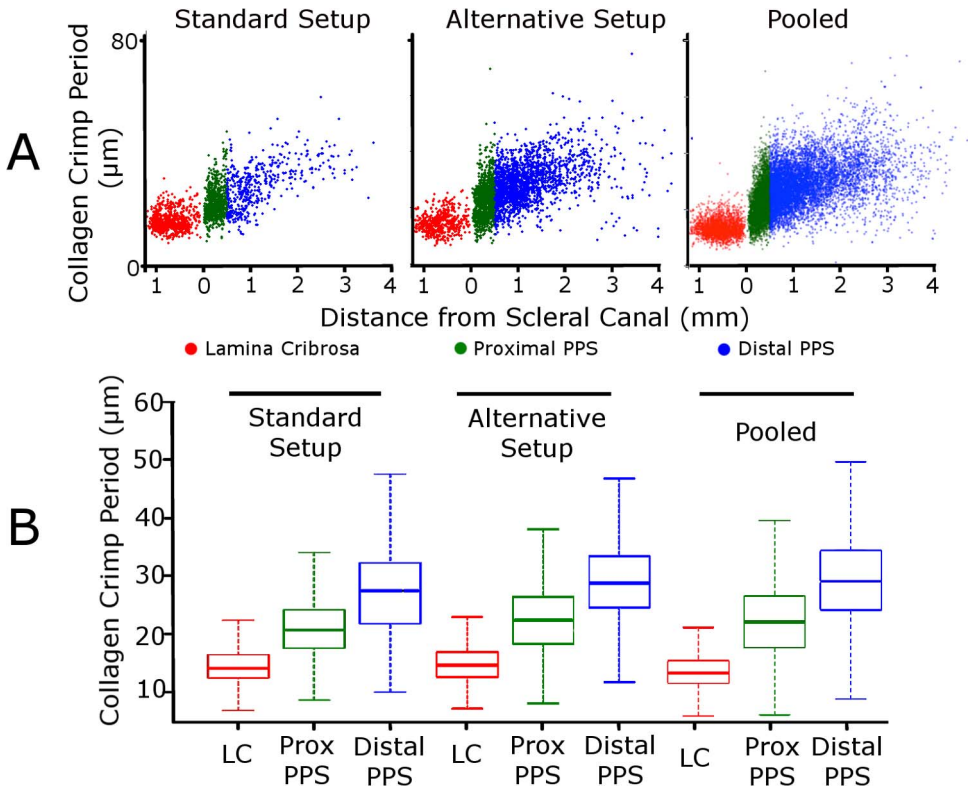


**Figure 5.** Collagen crimp period scatterplots (**A**) and box plots (**B**) from using different imaging setups in two example eyes, and pooled across seven eyes fixed at 5-mm Hg IOP. The *left side* corresponds with the standard setup (Olympus–Olympus microscope–camera pairing), the middle with the alternative imaging setup (as defined in the main text), and the *right side* with the pooled distributions across seven eyes. The period measurements were robust to using different microscope–camera pairings and similar between different eyes and animals.

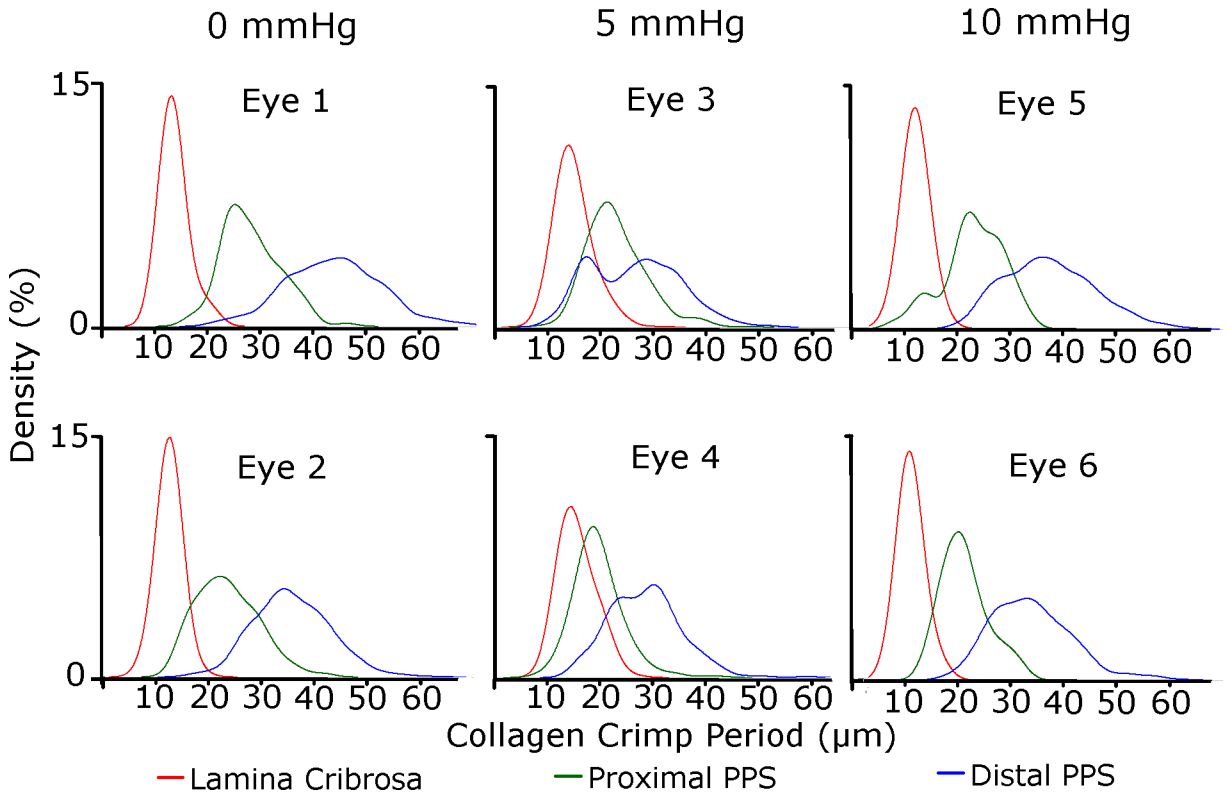


FIGURE 6. Density plots of the collagen crimp period distribution in each eye by LC and PPS regions.

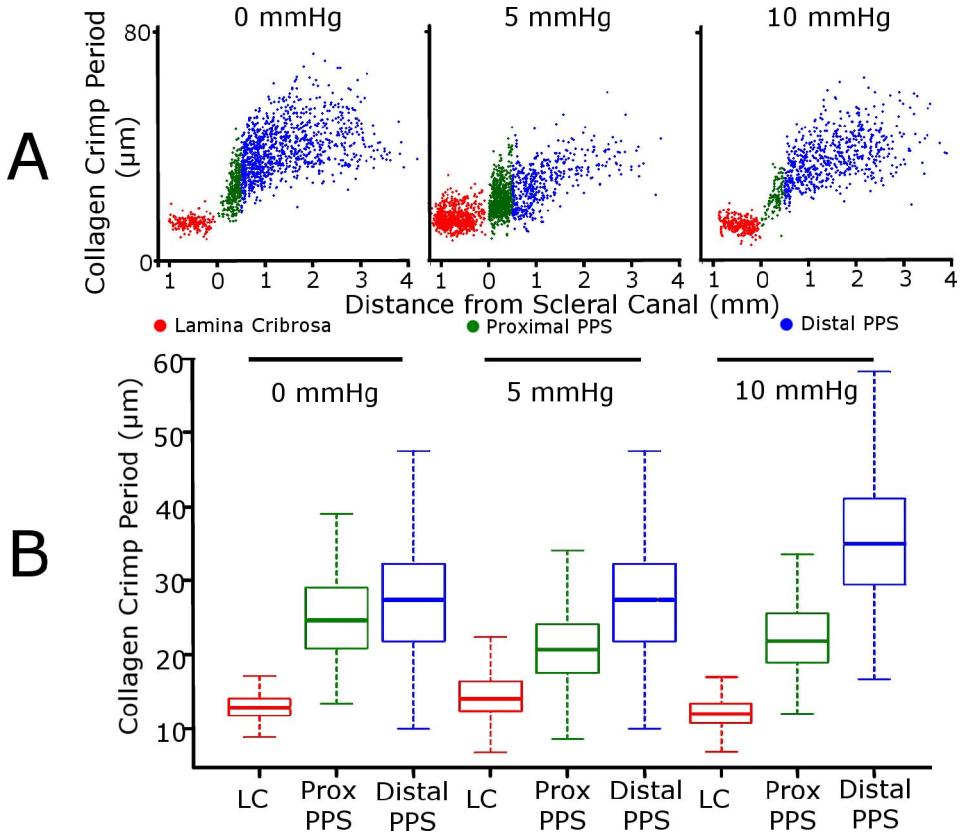


FIGURE 7. Scatterplots (A) and boxplots (B) of the collagen crimp period as a function of distance from the scleral canal pooling all sections and eyes at a given IOP. This distribution was similar between eyes fixed at different IOPs.

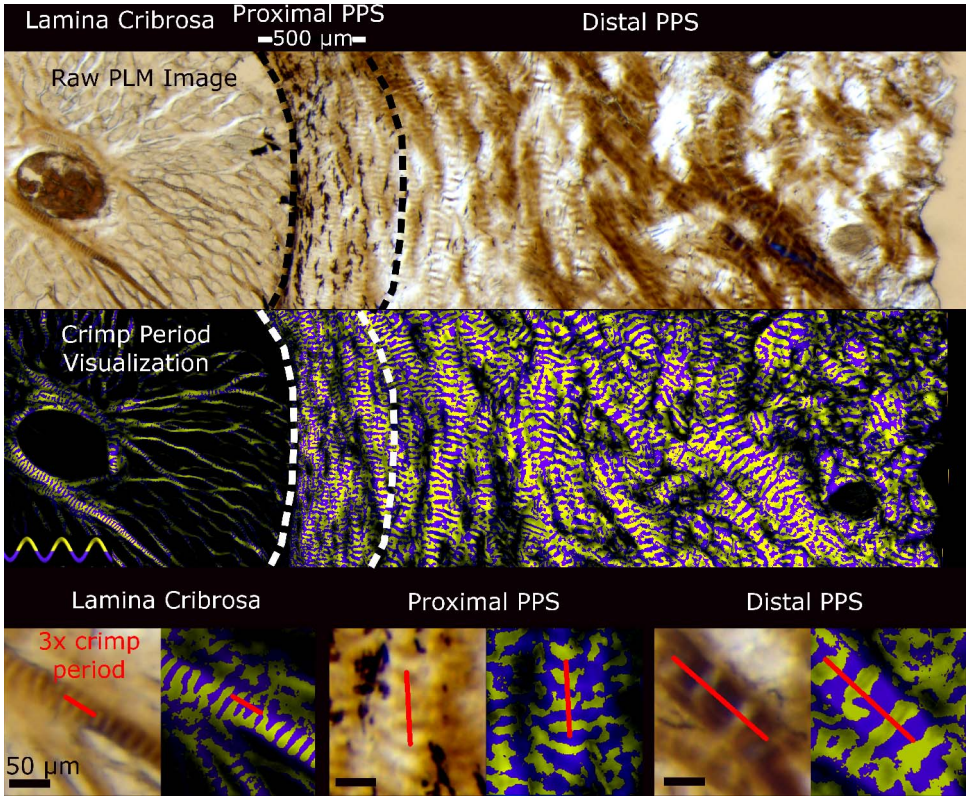


**Figure 8.** Wide views spanning the LC and sclera under PLM (*top*) and visualized using the *yellow* and *purple bands* as described in the text to simplify discerning crimp period independent of the orientation (*middle*). The *bottom* shows pairs of raw PLM images and corresponding crimp period visualization images of close-ups of the LC (*bottom left*), proximal PPS (*bottom center*), and distal PPS (*bottom right*). An example line illustrating three periods is overlaid on each. It is easy to distinguish that the crimp period in the LC was small. In the proximal PPS the period was similar to that of the LC. The period increased with distance from the canal.

way, the small differences in crimp period and variability between the proximal PPS and LC may reduce differences between the tissue stiffnesses at normal IOPs. This would alleviate concentrations of stress and strain, particularly shear, which are often harmful to tissues. At elevated IOPs, the heterogeneous crimp patterns would provide the PPS the ability to recruit additional fibers away from the canal, increasing tissue stiffness while still preventing large insult to the LC. We should note, however, that the direct mechanical relationship between crimp period and fiber recruitment and tissue stiffness remains unknown and should be investigated. One of the main motivations for this work was to provide experimental data on the baseline crimp characteristics needed for the development of robust fiber-based microstructure constitutive models of the LC and PPS.

**Table.** Summary of Results From Statistical Tests

| | Lamina Cribrosa | | Peripapillary Sclera | |
|---|---|---|---|---|
| **Model Type** | **AIC** | ***P* Value** | **AIC** | ***P* Value** |
| Linear | 5744 | 0.6468 | 22358 | <0.0001 |
| Log | 5732 | 0.8907 | 22319 | <0.0001 |
| Square Root | 5737 | 0.7659 | **22158** | **<0.0001** |

The distance was transformed according to the model type and the AIC and *P* value was calculated to determine the best model. The bolded model was best for the PPS, with the lowest AIC and a significant *P* value.

We are not the first to report regional collagen structure heterogeneity in the ONH. However, most studies have lacked the sensitivity and resolution, or the field of view for measuring the collagen crimp that we have studied. The majority of past studies have focused on the macroscale patterns in the collagen structure. Ex vivo studies using serial block face imaging,[36] second harmonic generated imaging (SHG),[30,37,38] as well as in vivo studies using optical coherence tomography (OCT)[39–41] have quantified LC trabeculae beam thicknesses and pore diameters, which was useful for understanding regional differences in the LC collagen macrostructure, but provide no information on collagen microstructure. For the PPS, studies using wide-angle x-ray scattering (WAXS)[5,42] and small angle light scattering (SALS)[7] quantified collagen fiber orientation patterns across large patches of ONH as well as for whole eye globes. Both techniques have visualized important patterns in the PPS collagen macrostructure, including a circumferential ring of collagen fibers around the scleral canal.[5,43–46] However, these studies did not address the collagen microstructure of the PPS either. One of the main reasons such modalities have not been able to detect microstructural crimp is that the orientation information that is quantified from SALS and WAXS combine the contributions of large-scale fiber bundle splay and microstructural crimp when measuring the collagen fiber angular distribution.[47] Therefore, a modality with higher sensitivity and resolution is needed to separate out these two contributions. Utilizing polarization-sensitive OCT, Baumann and colleagues[48] noted a donut-shaped pattern of scleral birefringence in the rat PPS, formed by circumferentially organized fibers.

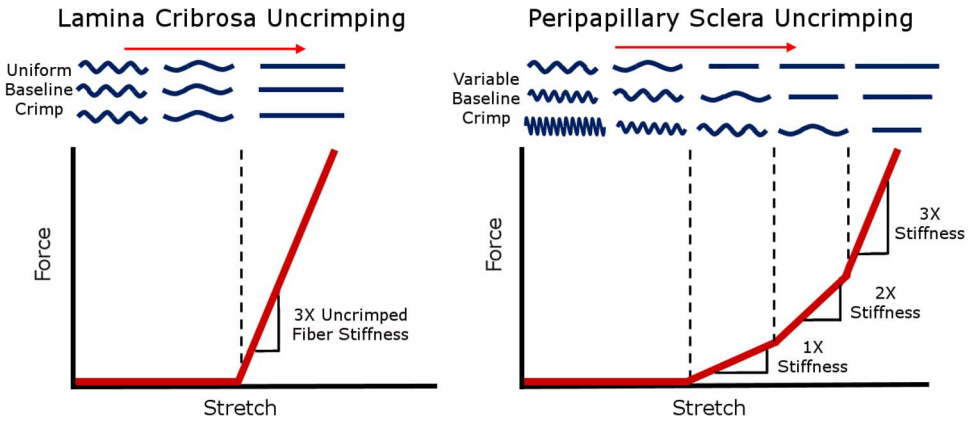


**Figure 9.** Schematic of how different baseline crimp distributions in the ONH can determine the nonlinear macroscopic biomechanical behavior of the tissue. In a region with uniform, such as the LC, base crimp distribution, stretch leads to a macroscopic step increase in stiffness due to the simultaneous straightening of the fibers. In a region with variable crimp distribution, such as the PPS, the variable crimp disribution results in a macroscopic gradual increase in stiffness with stretch. It is important to note that crimp period is only one aspect of the fiber undulation and other characteristics could vary differently.

Many of the imaging techniques mentioned above are more appropriate to one tissue or the other due to large differences in the tissue density and feature size between the LC and PPS. In comparison, PLM has the appropriate sensitivity and resolution to quantify crimp in both individual LC beams and PPS collagen bundles creating a fair basis for comparison.

The relationship between crimp morphology and the overall mechanical properties of tissue is very complex. In this work we have focused on the crimp period, a natural property of the wavy or undulating collagen fibers. Nevertheless, it is important to remember that crimp period is only one aspect of the fiber undulation. Other aspects of crimp, such as the maximum deviation angle, amplitude, tortuosity, and waviness can also be used to characterize the crimp, and could vary in different ways than period. For example, two different collagen fibers can have the same crimp period, but different waviness or amplitude. Because of this, a larger or smaller crimp period may not indicate tissue that is less or more stretched, respectively. However, there may be some redundancy between the parameters and not all may be needed to fully characterize the undulations. Grytz and colleagues[22] used inverse modeling to predict the crimp maximum deviation angle in the ONH, whereas others have measured the amplitude of fibers in the pulmonary valve,[49] and the tortuosity of fibers in ventricular myocardium.[50] Although it is generally accepted that as fibers are stretched, they will lose their crimp, each crimp parameter may have a different relationship with stretch. Further research is needed to quantify additional crimp characteristics to be able to predict local fiber recruitment and tissue properties under various levels of IOP.

The collagen in the eye has also been visualized, even if not systematically analyzed and measured.[14–16,19,51,52] Electron micrographs revealed the wavy collagen fiber crimp in the cornea more than 30 years ago.[15] Since then, others have visualized the crimp in the eye with other imaging modalities, including brightfield,[14] nonlinear microscopy,[51] and MRI.[19] Experimental measures of crimp characteristics exist for the cornea, using transmission electron microscopy,[23] but not for the LC or sclera.

A useful property of the technique we have presented, is that the sample preparation is relatively simple. Using PLM, collagenous tissue is visible without stains or labels, avoiding time-consuming multistep procedures. Crimp features are orientation-sensitive, so manually measuring the crimp period from sections imaged with PLM is intuitive, in comparison to measuring period from strained sections imaged with bright-field microscopy or labeled sections imaged with fluorescence microscopy.[53–58] Our technique also minimizes tissue processing, reducing potential artifacts. The tissues were never dehydrated, a step necessary in paraffin or plastic embedding which shrinks and warps tissue. The tissues were also never flattened, a common practice when studying scleral tissue with SALS[7] or WAXS[44] that could affect the collagen structure and bias orientation measurements.

Along with the strengths of our method, it is important to also consider its limitations. There are potential artifacts from using ex vivo tissues, histologic processing, and cryosectioning. The tissues may have artifacts from 10% formalin fixation, though we have shown our method of fixation has minimal effects on ocular tissue size or shape (Tran H, manuscript submitted, 2017). It is also possible that there existed some shell distortion for the eyes fixed at 0-mm Hg IOP, which could have deformed the collagen affecting the crimp period measured. However, we did not detect any statistically significant differences in crimp period between eyes fixed at 0-, 5-, or 10-mm Hg IOP, so the effects were small relative to the variability. Other crimp parameters may be more sensitive to these changes with IOP. Future studies could address other general structural artifacts by using fiducial markers to correct for tissue warping during processing and sectioning.[58] Another limitation is the use of sheep eyes. Sheep eyes, like human eyes, have a collagenous LC. However, there are distinct structural differences, including a thick tree-like structure called the ventral groove in the ONH. It is possible that the microstructural crimp patterns we found in sheep may not apply to humans. It is important to understand sheep as an animal model,[59] but future work should include measurements of crimp in other animal models as well as human.

Our measurements of the crimp period were done in two dimensions in coronal sections of the ONH. It is possible that the direction of sectioning may affect the collagen crimp period measurements. This could be addressed, for example, through the development of techniques that permit measurement of collagen orientation in three dimensions (3D) (Yang B, et al. *IOVS* 2017;58:ARVO E-Abstract 4825). However, in the ONH, the tissue is mainly loaded in the coronal direction. Biomechanical studies have shown that even though the IOP acts normal to the tissue, the main direction of loading (i.e., the largest forces) is in the transverse direction.[60–62] Because of

this preferential loading direction, the fibers oriented in this plane bear these loads and largely determine the biomechanics of the eye. Because our measurements were from coronal, or transverse, sections in the preferred loading direction, the in-plane crimp periods are most relevant and the fibers on which these were measured are more likely to have large in-plane components. Also, the crimp period measurements we obtained may be affected by the angle of a bundle relative to the plane of the section. As such, our measurements would be projections of 3D periods, and therefore could underestimate the actual bundle periods. Thus, it seems reasonable to expect that measurements obtained in 3D would still show lower crimp periods in the LC than in the PPS. Nevertheless, this must be confirmed.

The crimp periods reported in this manuscript were cross-sectional, where the crimp in each eye was measured at a specific IOP. Because of this, the crimp trends reported are a reflection of a population of collagen fibers, rather than any specific fiber and how the crimp in a single fiber would change with pressure. To obtain this information, future studies could explore a different type of experimental design, for example, tracking effects of loading on specific fibers or bundles (Jan NJ, et al. *IOVS* 2016;57:ARVO E-Abstract 3566).

In conclusion, to the best of our knowledge, we have presented the first systematic experimental characterization of the collagen crimp in the ONH. Crimp characteristics are important because they largely determine the nonlinear biomechanical behavior of the tissues. Our period measurements provide a basis to understand how microstructure governs larger scale tissue mechanics. This information helps reveal the role of microstructure on eye physiology, in aging, and in biomechanics-related diseases, such as glaucoma. Future directions include measuring other characteristics of the collagen crimp in addition to the period, as well as how these characteristics change with mechanical stimuli such as changes in IOP.

## *Acknowledgments*

The authors thank Jonathan Constantin, Michael Iasella, Sarah Smelko, Ryan O'Malley, Natalie Rutkowski, Tyler Martin, and Michael Urich for making the measurements analyzed in this study. They also thank Katharine Davoli for help with histology.

Supported by grants from the National Institutes of Health R01-EY023966, R01-EY013178, R01-EY025011, T32-EY017271, and P30-EY008098 (Bethesda, MD, USA), and the Eye and Ear Foundation (Pittsburgh, PA, USA).

Disclosure: **N.-J. Jan**, None; **C. Gomez**, None; **S. Moed**, None; **A.P. Voorhees**, None; **J.S. Schuman**, P; **R.A. Bilonick**, None; **I.A. Sigal**, None

## *References*

1. Fratzl P. *Collagen: Structure and Mechanics*. New York City, NY: Springer Science & Business Media; 2008.
2. Wainwright SA, Biggs W, Currey J, Gosline J. *Mechanical Design in Organisms*. Princeton: Princeton University Press; 1982.
3. Niklas KJ. *Plant Biomechanics: An Engineering Approach to Plant Form and Function*. Chicago: University of Chicago Press; 1992.
4. Mattheck C. *Design in Nature: Learning From Trees*. Berlin: Springer-Verlag Berlin Heidelberg; 1998.
5. Pijanka JK, Coudrillier B, Ziegler K, et al. Quantitative mapping of collagen fiber orientation in non-glaucoma and glaucoma posterior human sclerae. *Invest Ophthalmol Vis Sci*. 2012;53:5258–5270.
6. Kamma-Lorger CS, Boote C, Hayes S, et al. Collagen and mature elastic fibre organisation as a function of depth in the human cornea and limbus. *J Struct Biol*. 2010;169:424–430.
7. Girard MJ, Dahlmann-Noor A, Rayapureddi S, et al. Quantitative mapping of scleral fiber orientation in normal rat eyes. *Invest Ophthalmol Vis Sci*. 2011;52:9684–9693.
8. Winkler M, Jester B, Nien-Shy C, et al. High resolution three-dimensional reconstruction of the collagenous matrix of the human optic nerve head. *Brain Res Bull*. 2010;81:339–348.
9. Holzapfel GA. Biomechanics of soft tissue. In: Lemaitre J, ed., *Handbook of Materials Behavior Models*. San Diego, CA: Academic Press; 2001:1057–1073.
10. Ottani V, Raspanti M, Ruggeri A. Collagen structure and functional implications. *Micron*. 2001;32:251–260.
11. Bader AN, Pena A-M, van Voskuilen CJ, et al. Fast nonlinear spectral microscopy of in vivo human skin. *Biomed Opt Express*. 2011;2:365–373.
12. Birch HL, Thorpe CT, Rumian AP. Specialisation of extracellular matrix for function in tendons and ligaments. *Muscles Ligaments Tendons J*. 2013;3:12–22.
13. Franchi M, Raspanti M, Dell'Orbo C, et al. Different crimp patterns in collagen fibrils relate to the subfibrillar arrangement. *Connect Tissue Res*. 2008;49:85–91.
14. Ostrin LA, Wildsoet CF. Optic nerve head and intraocular pressure in the guinea pig eye. *Exp Eye Res*. 2016;146:7–16.
15. Andreo R, Farrell R. Corneal small-angle light-scattering theory: wavy fibril models. *J Opt Soc Am*. 1982;72:1479–1492.
16. Mega Y, Robitaille M, Zareian R, McLean J, Ruberti J, DiMarzio C. Quantification of lamellar orientation in corneal collagen using second harmonic generation images. *Opt Lett*. 2012;37:3312–3314.
17. Winkler M, Chai D, Kriling S, et al. Nonlinear optical macroscopic assessment of 3-d corneal collagen organization and axial biomechanics. *Invest Ophthalmol Vis Sci*. 2011;52:8818–8827.
18. Midgett DE, Quigley HA, Pease ME, Franck C, Toyjanova J, Nguyen TD. Inflation test of the human optic nerve head using digital volume correlation. In: Tekalur SA, Zavattieri P, Korach CS, eds. *Mechanics of Biological Systems and Materials, Volume 6*. Orlando, FL: Springer; 2016:7–15.
19. Ho LC, Sigal IA, Jan N-J, et al. Magic angle–enhanced MRI of fibrous microstructures in sclera and cornea with and without intraocular pressure loading. 2014;55:5662–5672.
20. Grytz R, Meschke G. Constitutive modeling of crimped collagen fibrils in soft tissues. *J Mech Behav Biomed Mater*. 2009;2:522–533.
21. Grytz R, Meschke G. A computational remodeling approach to predict the physiological architecture of the collagen fibril network in corneo-scleral shells. *Biomech Model Mechanobiol*. 2010;9:225–235.
22. Grytz R, Meschke G, Jonas JB. The collagen fibril architecture in the lamina cribrosa and peripapillary sclera predicted by a computational remodeling approach. *Biomech Model Mechanobiol*. 2011;10:371–382.
23. Liu X, Wang L, Ji J, et al. A mechanical model of the cornea considering the crimping morphology of collagen fibrils. *Invest Ophthalmol Vis Sci*. 2014;55:2739–2746.
24. Ghaffari MS, Shojaei M, Sabzevari A, Khorami N. Reference values for intraocular pressure and schirmer tear test in clinically normal sanjabi sheep. *Small Ruminant Res*. 2011;97:101–103.
25. Jan N-J, Grimm JL, Tran H, et al. Polarization microscopy for characterizing fiber orientation of ocular tissues. *Biomed Opt Express*. 2015;6:4705–4718.
26. Jan N-J, Lathrop K, Sigal IA. Collagen architecture of the posterior pole: high-resolution wide field of view visualization

and analysis using polarized light microscopy. *Invest Ophthalmol Vis Sci*. 2017;58:735–744.

27. Preibisch S, Saalfeld S, Tomancak P. Globally optimal stitching of tiled 3d microscopic image acquisitions. *Bioinformatics*. 2009;25:1463–1465.
28. Schindelin J, Arganda-Carreras I, Frise E, et al. Fiji: an open-source platform for biological-image analysis. *Nat Methods*. 2012;9:676–682.
29. Diamant J, Keller A, Baer E, Litt M, Arridge R. Collagen; ultrastructure and its relation to mechanical properties as a function of ageing. *Proc R Soc Lond B Biol Sci*. 1972;180:293–315.
30. Sigal IA, Grimm JL, Jan N-J, Reid K, Minckler DS, Brown DJ. Eye-specific IOP-induced displacements and deformations of human lamina cribrosa. *Invest Ophthalmol Vis Sci*. 2014;55:1–15.
31. Voorhees AP, Jan N-J, Sigal IA. Effects of collagen microstructure and material properties on the deformation of the neural tissues of the lamina cribrosa [published online ahead of print May 18, 2017]. *Acta Biomater*. 2017. doi:10.1016/j.actbio.2017.05.042.
32. Franchi M, Fini M, Quaranta M, et al. Crimp morphology in relaxed and stretched rat achilles tendon. *J Anat*. 2007;210:1–7.
33. Wang R, Raykin J, Gleason RL Jr, Ethier CR. Residual deformations in ocular tissues. *J R Soc Interface*. 2015; 12: pii 20141101.
34. Woo SLY, Kobayashi AS, Schlegel WA, Lawrence C. Nonlinear material properties of intact cornea and sclera. *Exp Eye Res*. 1972;14:29–39.
35. Voorhees A, Millwater H, Bagley R. Complex variable methods for shape sensitivity of finite element models. *Finite Elem Anal Des*. 2011;47:1146–1156.
36. Reynaud J, Lockwood H, Gardiner SK, Williams G, Yang H, Burgoyne CF. Lamina cribrosa microarchitecture in monkey early experimental glaucoma: global change. *Invest Ophthalmol Vis Sci*. 2016;57:3451–3469.
37. Albon J, Farrant S, Akhtar S, et al. Connective tissue structure of the tree shrew optic nerve and associated ageing changes. *Invest Ophthalmol Vis Sci*. 2007;48:2134–2144.
38. Brown DJ, Morishige N, Neekhra A, Minckler DS, Jester JV. Application of second harmonic imaging microscopy to assess structural changes in optic nerve head structure ex vivo. *J Biomed Opt*. 2007;12:024029.
39. Wang B, Nevins JE, Nadler Z, et al. In vivo lamina cribrosa micro-architecture in healthy and glaucomatous eyes as assessed by optical coherence tomographyin vivo assessment of 3d LC micro-architecture. *Invest Ophthalmol Vis Sci*. 2013;54:8270–8274.
40. Ivers KM, Li C, Patel N, et al. Reproducibility of measuring lamina cribrosa pore geometry in human and nonhuman primates with in vivo adaptive optics imaging. *Invest Ophthalmol Vis Sci*. 2011;52:5473–5480.
41. Nadler Z, Wang B, Wollstein G, et al. Automated lamina cribrosa microstructural segmentation in optical coherence tomography scans of healthy and glaucomatous eyes. *Biomed Opt Express*. 2013;4:2596–2608.
42. Coudrillier B, Pijanka J, Jefferys J, et al. Collagen structure and mechanical properties of the human sclera: analysis for the effects of age. *J Biomech Eng*. 2015;137:041006.
43. Pijanka JK, Spang MT, Sorensen T, et al. Depth-dependent changes in collagen organization in the human peripapillary sclera. *PLoS One*. 2015;10:e0118648.
44. Pijanka JK, Abass A, Sorensen T, Elsheikh A, Boote C. A wide-angle x-ray fibre diffraction method for quantifying collagen orientation across large tissue areas: application to the human eyeball coat. 2013;46:1481–1489.
45. Thale A, Tillmann B. The collagen architecture of the sclera–sem and immunohistochemical studies. *Ann Anat*. 1993;175:215–220.
46. Quigley HA, Dorman-Pease ME, Brown AE. Quantitative study of collagen and elastin of the optic nerve head and sclera in human and experimental monkey glaucoma. *Curr Eye Res*. 1991;10:877–888.
47. Pierlot CM, Lee JM, Amini R, Sacks MS, Wells SM. Pregnancy-induced remodeling of collagen architecture and content in the mitral valve. *Ann Biomed Eng*. 2014;42:2058–2071.
48. Baumann B, Rauscher S, Glösmann M, et al. Peripapillary rat sclera investigated in vivo with polarization-sensitive optical coherence tomography. *Invest Ophthalmol Vis Sci*. 2014;55:7686–7696.
49. Joyce EM, Liao J, Schoen FJ, Mayer JE Jr, Sacks MS. Functional collagen fiber architecture of the pulmonary heart valve cusp. *Ann Thorac Surg*. 2009;87:1240–1249.
50. Omens JH, Miller TR, Covell JW. Relationship between passive tissue strain and collagen uncoiling during healing of infarcted myocardium. *Cardiovasc Res*. 1997;33:351–358.
51. Quantock AJ, Winkler M, Parfitt GJ, et al. From nano to macro: studying the hierarchical structure of the corneal extracellular matrix. *Exp Eye Res*. 2015;133:81–99.
52. Meek KM, Boote C. The use of x-ray scattering techniques to quantify the orientation and distribution of collagen in the corneal stroma. *Prog Retin Eye Res*. 2009;28:369–392.
53. Hernandez MR, Andrzejewska WM, Neufeld AH. Changes in the extracellular matrix of the human optic nerve head in primary open-angle glaucoma. *Am J Ophthalmol*. 1990;109:180–188.
54. Hernandez MR, Luo XX, Andrzejewska W, Neufeld AH. Age-related changes in the extracellular matrix of the human optic nerve head. *Am J Ophthalmol*. 1989;107:476–484.
55. Hernandez MR, Luo XX, Igoe F, Neufeld AH. Extracellular matrix of the human lamina cribrosa. *Am J Ophthalmol*. 1987;104:567–576.
56. Downs JC, Yang H, Girkin C, et al. Three-dimensional histomorphometry of the normal and early glaucomatous monkey optic nerve head: neural canal and subarachnoid space architecture. *Invest Ophthalmol Vis Sci*. 2007;48:3195–3208.
57. Yang H, Downs JC, Bellezza A, Thompson H, Burgoyne CF. 3-D histomorphometry of the normal and early glaucomatous monkey optic nerve head: prelaminar neural tissues and cupping. *Invest Ophthalmol Vis Sci*. 2007;48:5068–5084.
58. Sigal IA, Flanagan JG, Tertinegg I, Ethier CR. 3D morphometry of the human optic nerve head. *Exp Eye Res*. 2010;90:70–80.
59. Gerometta R, Spiga M-G, Borrás T, Candia OA. Treatment of sheep steroid–induced ocular hypertension with a glucocorticoid-inducible mmp1 gene therapy virus. *Invest Ophthalmol Vis Sci*. 2010;51:3042–3048.
60. Bellezza AJ, Hart RT, Burgoyne CF. The optic nerve head as a biomechanical structure: initial finite element modeling. *Invest Ophthalmol Vis Sci*. 2000;41:2991–3000.
61. Sigal IA, Flanagan JG, Tertinegg I, Ethier CR. Finite element modeling of optic nerve head biomechanics. *Invest Ophthalmol Vis Sci*. 2004;45:4378–4387.
62. Norman RE, Flanagan JG, Sigal IA, Rausch SM, Tertinegg I, Ethier CR. Finite element modeling of the human sclera: influence on optic nerve head biomechanics and connections with glaucoma. *Exp Eye Res*. 2011;93:4–12.

Investigative Ophthalmology & Visual Science